Multicritical Nishimori point in the phase diagram of the $\pm J$ Ising model on a square lattice

Martin Hasenbusch,[1] Francesco Parisen Toldin,[2] Andrea Pelissetto,[3] and Ettore Vicari[4]
[1]*Institut für Theoretische Physik, Universität Leipzig, Postfach 100 920, D-04009 Leipzig, Germany*
[2]*Max-Planck-Institut für Metallforschung, Heisenbergstrasse 3, D-70569 Stuttgart, Germany*
and Institut für Theoretische und Angewandte Physik, Universität Stuttgart, Pfaffenwaldring 57, D-70569 Stuttgart, Germany
[3]*Dipartimento di Fisica dell'Università di Roma "La Sapienza" and INFN, Piazzale Aldo Moro 2, I-00185 Roma, Italy*
[4]*Dipartimento di Fisica dell'Università di Pisa and INFN, Largo Pontecorvo 3, I-56127 Pisa, Italy*
(Received 8 March 2008; published 15 May 2008)

We investigate the critical behavior of the random-bond $\pm J$ Ising model on a square lattice at the multicritical Nishimori point in the T-p phase diagram, where T is the temperature and p is the disorder parameter ($p=1$ corresponds to the pure Ising model). We perform a finite-size scaling analysis of high-statistics Monte Carlo simulations along the Nishimori line defined by $2p-1=\tanh(1/T)$, along which the multicritical point lies. The multicritical Nishimori point is located at $p^*=0.890\ 81(7)$, $T^*=0.9528(4)$, and the renormalization-group dimensions of the operators that control the multicritical behavior are $y_1=0.655(15)$ and $y_2=0.250(2)$; they correspond to the thermal exponent $\nu\equiv 1/y_2=4.00(3)$ and to the crossover exponent $\phi\equiv y_1/y_2=2.62(6)$.

DOI: 10.1103/PhysRevE.77.051115 PACS number(s): 64.60.Kw, 75.10.Nr, 75.40.Cx, 75.40.Mg

I. INTRODUCTION

The $\pm J$ Ising model on a square lattice represents an interesting theoretical laboratory in which one can study the effects of quenched disorder and frustration on the critical behavior of two-dimensional (2D) spin systems. It is defined by the lattice Hamiltonian

$$\mathcal{H} = -\sum_{\langle xy\rangle} J_{xy}\sigma_x\sigma_y, \tag{1}$$

where $\sigma_x=\pm 1$, the sum is over pairs of nearest-neighbor sites of a square lattice, and the exchange interactions J_{xy} are uncorrelated quenched random variables, taking values $\pm J$ with probability distribution

$$P(J_{xy}) = p\,\delta(J_{xy}-J) + (1-p)\,\delta(J_{xy}+J). \tag{2}$$

In the following we set $J=1$ without loss of generality. For $p=1$ we recover the standard Ising model, while for $p=1/2$ we obtain the bimodal Ising spin-glass model. The $\pm J$ Ising model is a simplified model [1] for disordered spin systems showing glassy behavior in some region of their phase diagram. The random nature of the short-ranged interactions is mimicked by nearest-neighbor random bonds. The 2D $\pm J$ Ising model is also interesting for the description of quantum Hall transitions [2–4], and for its applications in coding theory [5–8].

The T-p phase diagram of the 2D $\pm J$ Ising model is sketched in Fig. 1 (it is symmetric for $p\to 1-p$ and thus we only report it for $1-p<1/2$). It has been investigated and discussed in several works, see, e.g., Refs. [2,5,8–29]. For sufficiently small values of the probability of antiferromagnetic bonds, the model presents a paramagnetic phase and a ferromagnetic phase, separated by a transition line. The paramagnetic-ferromagnetic (PF) transition line starts at the Ising point $X_{\rm Is}=(T=T_{\rm Is},p=1)$, where $T_{\rm Is}=2/\ln(1+\sqrt{2})=2.269\ 19\ldots$ is the critical temperature of the 2D Ising model, and extends up to the multicritical Nishimori point (MNP) at $X_{\rm MNP}=(T^*,p^*)$, with $T^*\approx 0.95$ and $p^*\approx 0.89$. Along this line, the critical behavior is analogous to that observed in 2D randomly dilute Ising (RDI) models [30–33]. It is controlled by the pure Ising fixed point and disorder is marginally irrelevant, giving rise to universal logarithmic corrections, as shown in Refs. [33,34]. As argued in Refs. [35–37], the MNP is located along the so-called Nishimori line (N line) [8,38] defined by the equation

$$\tanh\beta = 2p-1, \tag{3}$$

where $\beta\equiv 1/T$. As a consequence of the inequality [38]

$$|[\langle\sigma_x\sigma_y\rangle_T]| \le [|\langle\sigma_x\sigma_y\rangle_{T_N(p)}|] \tag{4}$$

(the angular and the square brackets refer, respectively, to the thermal average and to the quenched average over the bond couplings $\{J_{xy}\}$, while the subscripts indicate the temperature of the thermal average), ferromagnetism can only exist in the region $p\ge p^*$, and the system is maximally magnetized along the N line. This implies that the PF boundary lies in the region $p\ge p^*$. At the MNP the transition line is predicted to be parallel to the T axis [37]. Then, it reaches the $T=0$ axis at $X_c=(0,p_c)$. As a consequence of inequality (4), p_c must satisfy the inequality

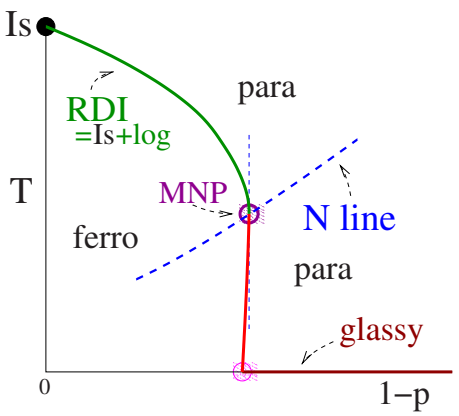

FIG. 1. (Color online) Phase diagram of the square-lattice $\pm J$ Ising model in the T-p plane.

$$p_c \geq p^*. \tag{5}$$

At variance with the three-dimensional case, there is no evidence of a finite-temperature glassy phase. Glassy behavior is only expected for $T=0$ and $p<p_c$: the glassy phase at $T=0$ is unstable with respect to thermal fluctuations. In Refs. [8,26,27,29] it was argued that the PF transition line that connects the MNP to X_c is only related to the frustration distribution; hence it should not depend on temperature and should coincide with the line $p=p^*$, so that $p_c=p^*$. This argument provides a good approximation of the phase diagram below the MNP, although it is not exact. Indeed, numerical analyses [5,10,12,16,22,24] clearly support a reentrant phase transition line with $p_c>p^*$. The difference is, however, quite small, $p_c-p^*\approx 0.006$.

The critical behavior along the transition line connecting the MNP to the $T=0$ axis is an open issue. Even though it separates a paramagnetic phase from a ferromagnetic phase, it seems unlikely that such transitions belong to the same universality class as the PF transitions that occur on the line connecting the Ising point to the MNP. They may be of first order (in this case the MNP would be a tricritical point) or continuous, but in a different universality class. The glassy transitions at $T=0$ and $p<p_c$ are expected to belong to the same universality class as that of the bimodal model with $p=1/2$, see, e.g., Ref. [39] and references therein. It is worth noting that the point $X_c=(0,p_c)$ is a multicritical point: it is connected to three phases and it is the intersection of two different transition lines, the PF line at $T>0$ and the glassy line at $T=0$. For $T=0$ the critical point X_c separates a ferromagnetic phase from a glassy phase, while for $T>0$ the transition line separates a ferromagnetic from a paramagnetic phase. Therefore if the line from the MNP to X_c corresponds to continuous transitions, the critical behavior at $T=0$ should differ from that at $T>0$ along the transition line from the MNP to X_c. The behavior in a neighborhood of the multicritical point X_c depends on the nature of the transition. If the PF transition and the glassy transition are effectively decoupled, we expect a phase diagram like that reported in Fig. 1. On the other hand, if the critical modes are coupled at X_c, all transition lines should be tangent at the multicritical point. Hence the PF line is expected to by tangent to the glassy transition line $T=0$.

Recently, Ref. [17] put forward an interesting conjecture concerning the location of the MNP in a general class of models in generic dimension. In the case of the 2D $\pm J$ model it predicts the MNP at

$$X_e \equiv (T_e = 0.956\,729\ldots, p_e = 0.889\,972\ldots). \tag{6}$$

The available numerical results show that Eq. (6) is a very good approximation of the location of the MNP; for example, the transfer-matrix calculations reported in Refs. [10,16,18,20] give $p^*=0.8906(2)$, 0.8907(2), 0.8906(2), 0.8905(2), respectively. Actually, since the small difference $p^*-p_e\approx 0.0006$ corresponds at best to approximately three error bars, these numerical works do not conclusively rule it out [9]. The conjecture has also been tested on hierarchical lattices. If is found that it is not exact, although discrepancies are also in this case numerically small [40,41].

In this paper we consider the square-lattice $\pm J$ model, determine the location of the MNP, and study the critical behavior in its vicinity. For this purpose, we perform high-statistics Monte Carlo (MC) simulations along the N line close to the MNP. We consider lattices of size L^2 with $6\leq L\leq 64$. A detailed finite-size scaling (FSS) analysis allows us to determine the location of the MNP quite precisely. We obtain

$$X_{\rm MNP} = [T^* = 0.9528(4), p^* = 0.890\,81(7)]. \tag{7}$$

We determine the renormalization-group (RG) dimensions y_1 and y_2 of the relevant operators that control the RG flow close to the MNP. We obtain $y_1=0.655(15)$ and $y_2=0.250(2)$, corresponding to the temperature and crossover exponents $\nu\equiv 1/y_2=4.00(3)$ and $\phi\equiv y_1/y_2=2.62(6)$, respectively. Our results confirm that X_e defined in Eq. (6) is a very good approximation of the MNP location: indeed, $p^*-p_e=0.000\,84(7)$. However, they also show that the conjecture of Ref. [17] leading to X_e is not exact.

The paper is organized as follows. In Sec. II we summarize the theoretical results, focusing in particular on the FSS behavior expected at the MNP. In Sec. III we present the FSS analysis of high-statistics MC simulations along the N line. In Sec. IV we summarize our results and draw our conclusions. In the Appendix we report some notations.

II. FINITE-SIZE SCALING AT THE MULTICRITICAL POINT

In the absence of external fields, the critical behavior at the MNP is characterized by two relevant RG operators. The singular part of the disorder-averaged free energy in a volume L^d can be written as

$$F_{\rm sing}(T,p,L) = L^{-d} f(u_1 L^{y_1}, u_2 L^{y_2}, \{u_i L^{y_i}\}), \quad i \geq 3, \tag{8}$$

where $y_1>y_2>0$, $y_i<0$ for $i\geq 3$, u_i are the corresponding scaling fields, $u_1=u_2=0$ at the MNP, and d is the space dimension ($d=2$ in the present case). In the infinite-volume limit and neglecting subleading corrections, we have

$$F_{\rm sing}(T,p) = |u_2|^{d/y_2} f_\pm(u_1|u_2|^{-\phi}), \quad \phi \equiv y_1/y_2 > 1, \tag{9}$$

where the functions $f_\pm(x)$ apply to the parameter regions in which $\pm u_2>0$. Close to the MNP, the transition lines correspond to constant values of the product $u_1|u_2|^{-\phi}$ and thus, since $\phi>1$, they are tangent to the line $u_1=0$.

The scaling fields u_i are analytic functions of the model parameters T and p. Using symmetry arguments, Refs. [36,37] showed that one of the scaling axes is along the N line, i.e., that the N line is either tangent to the line $u_1=0$ or to $u_2=0$. Since the N line cannot be tangent to the transition lines at the MNP and these lines are tangent to $u_1=0$, the first possibility is excluded. Thus close to the MNP the N line corresponds to $u_2=0$. Thus we identify [36,37]

$$u_2 = \tanh\beta - 2p + 1. \tag{10}$$

As for the scaling axis $u_1=0$, $\epsilon\equiv 6-d$ expansion calculations predict it [37] to be parallel to the T axis. The extension of this result to lower dimensions suggests

TABLE I. Parameters of our random-exchange MC runs. N_{run} is the number of Metropolis sweeps per configuration and sample, N_{therm} is the corresponding number of Metropolis sweeps discarded for thermalization.

L	p	β_{min}	N_T	Acceptance range (%)	$N_{\mathrm{run}}/10^3$	$N_{\mathrm{therm}}/10^3$
32	0.8895	0.3228	13	4–56	240	48
32	0.889972	0.3252	13	4–56	240	48
32	0.8905	0.3279	13	4–56	240	48
32	0.8910	0.3305	13	4–57	240	72
32	0.8915	0.3331	13	4–57	240	48
48	0.889972	0.285228	20	4–57	400	80
48	0.8905	0.2879	20	4–57	400	80
48	0.8910	0.2905	20	4–57	400	80
48	0.8915	0.3310	25	13–66	320	64
64	0.889972	0.265228	27	4–57	900	180
64	0.8906	0.268442	27	4–57	600	180
64	0.8909	0.2700	27	4–58	600	300
64	0.8909	0.2700	27	4–58	1200	240
64	0.8912	0.271529	27	4–58	600	240

$$u_1 = p - p^*. \tag{11}$$

Note that, if Eq. (11) holds, only the scaling field u_2 depends on the temperature T. We may then identify $\nu = 1/y_2$, and rewrite Eq. (9) as

$$F_{\mathrm{sing}}(T,p) = |t|^{2\nu} f_{\pm}(g|t|^{-\phi}), \tag{12}$$

where $t \equiv (T-T^*)/T^*$, $g \equiv p-p^*$, and ϕ is the crossover exponent.

These results give rise to the following predictions for the FSS behavior around T^*, p^*. Let us consider a RG invariant quantity R, such as $R_\xi \equiv \xi/L$, U_4, U_{22}, which are defined in the Appendix and called phenomenological couplings. In the FSS limit R obeys the scaling law

$$R = \mathcal{R}(u_1 L^{y_1}, u_2 L^{y_2}, \{u_i L^{y_i}\}), \quad i \geq 3. \tag{13}$$

Neglecting the scaling corrections, that is terms vanishing in the limit $L \to \infty$, very close to the MNP we expect

$$R = R^* + b_{11} u_1 L^{y_1} + b_{21} u_2 L^{y_2} + \cdots. \tag{14}$$

which is valid as long as $u_1 L^{y_1}$ is small. Along the N line, the scaling field u_2 vanishes, so that we can write

$$R_N = R^* + b_{11} u_1 L^{y_1} + \cdots, \tag{15}$$

where the subscript N indicates that R is restricted to the N line. Let us now consider the derivative of R with respect to $\beta \equiv 1/T$. Differentiating Eq. (14), we obtain

$$R' = b_{11} u_1' L^{y_1} + b_{21} u_2' L^{y_2} + \cdots. \tag{16}$$

If Eq. (11) holds, then $u_1' = 0$, so that

$$R' = b_{21} u_2' L^{y_2} + \cdots. \tag{17}$$

This result gives us a method to verify the conjecture of Ref. [37]: once y_1 has been determined from the scaling behavior of a RG invariant quantity close to the MNP, it is enough to check the scaling behavior of R'. If R' scales as L^ζ with $\zeta < y_1$, the conjecture is confirmed and ζ provides an estimate of y_2. Along the N line the magnetic susceptibility is expected to behave as

$$\chi_N = eL^{2-\eta}(1 + e_1 u_1 L^{y_1} + \cdots). \tag{18}$$

Let us mention that the general features of the MNP are expected to be independent of d. In three dimensions they have been accurately verified in Refs. [42,43].

III. MONTE CARLO RESULTS

A. Simulation details

In the following we present a FSS analysis of high-statistics MC data along the N line defined by

$$\beta = \beta_N(p) \equiv -\frac{1}{2}\ln\left(\frac{1-p}{p}\right). \tag{19}$$

We performed MC simulations on square lattices of linear size L with periodic boundary conditions, for several values of L, $L=6$, 8, 12, 16, 24, 32, 48, and 64. Most simulations were performed close to the MNP, for values of p in the range $0.8895 \leq p \leq 0.8920$, which includes the value $p_e = 0.889\,972\ldots$. To increase the statistics, we used multispin coding (details can be found in Ref. [44]).

We use a standard Metropolis algorithm up to $L=24$, while for $L \geq 32$ we supplement the updating method with the random-exchange technique [45] (see also Sec. 3 in Ref. [46] for a discussion of the random-exchange method in a disordered system). In order to determine MC estimates at p and $\beta = \beta_N(p)$, we consider N_T systems at the same value of p and at inverse temperatures $\beta_{\mathrm{min}} \equiv \beta_1, \ldots, \beta_{N_T} = \beta_N(p)$. The chosen values of β are equally spaced, i.e., $\beta_{i+1} - \beta_i = \Delta\beta$, with a constant $\Delta\beta$ (typically $\Delta\beta \approx 0.06$, 0.04, and 0.03 for $L=32$, 48, and 64). The spacing $\Delta\beta$ is chosen such as to

TABLE II. MC data for $L=6$, 8, 12, and 16 along the N line. For all runs the number of samples is $N_s=10^6$.

L	p	R_ξ	U_4	U_{22}	χ	R'_ξ
6	0.8895	0.9806(8)	1.1316(2)	0.08302(17)	26.172(8)	6.532(6)
	0.889972	0.9886(8)	1.1295(2)	0.08176(17)	26.270(8)	6.456(6)
	0.8905	0.9979(8)	1.1272(2)	0.08032(17)	26.382(8)	6.371(6)
	0.891	1.0068(8)	1.1250(2)	0.07899(17)	26.486(8)	6.290(6)
	0.8915	1.0158(8)	1.1229(2)	0.07765(17)	26.590(8)	6.210(6)
	0.892	1.0251(8)	1.1207(2)	0.07632(16)	26.695(8)	6.129(6)
8	0.8895	0.9741(7)	1.1327(2)	0.08455(17)	44.150(13)	13.471(11)
	0.889972	0.9837(7)	1.1301(2)	0.08301(16)	44.366(13)	13.307(11)
	0.8905	0.9945(7)	1.1274(2)	0.08132(16)	44.604(13)	13.126(11)
	0.891	1.0049(7)	1.1249(2)	0.07973(16)	44.829(13)	12.953(11)
	0.8915	1.0156(7)	1.1223(2)	0.07811(16)	45.054(12)	12.787(11)
	0.892	1.0265(8)	1.1198(2)	0.07654(16)	45.278(12)	12.615(11)
12	0.8895	0.9630(7)	1.1350(2)	0.08672(17)	91.98(3)	36.01(3)
	0.889972	0.9754(7)	1.1317(2)	0.08464(17)	92.61(3)	35.56(3)
	0.8905	0.9893(7)	1.1281(2)	0.08239(17)	93.31(3)	35.02(2)
	0.891	1.0030(7)	1.1247(2)	0.08028(16)	93.97(3)	34.52(2)
	0.8915	1.0167(8)	1.1214(2)	0.07821(16)	94.63(3)	34.04(2)
	0.892	1.0309(8)	1.1182(2)	0.07618(16)	95.29(3)	33.56(2)
16	0.8895	0.9554(7)	1.1373(2)	0.08840(16)	154.69(5)	71.09(4)
	0.889972	0.9701(7)	1.1333(2)	0.08587(16)	156.02(5)	70.15(4)
	0.8905	0.9870(7)	1.1289(2)	0.08311(16)	157.52(5)	69.11(4)
	0.891	1.0033(7)	1.1248(2)	0.08051(16)	158.92(5)	68.10(4)
	0.8915	1.0199(7)	1.1208(2)	0.07804(15)	160.31(4)	67.06(4)
	0.892	1.0367(8)	1.1170(2)	0.07562(15)	161.68(4)	66.03(4)

have a non-negligible acceptance probability, while $\beta_{\min}$ is chosen so that thermalization at $\beta=\beta_{\min}$ is sufficiently fast. The elementary unit of the algorithm consists in $N_{\rm ex}$ Metropolis sweeps for each configuration followed by an exchange move. We consider all pairs of configurations corresponding to nearby temperatures and propose a temperature exchange with acceptance probability

$$\mathcal{P}=\exp\{(\beta_i-\beta_{i+i})(E_i-E_{i+1})\}, \tag{20}$$

where E_i is the energy of the system at inverse temperature β_i. In our MC runs we choose $N_{\rm ex}=20$. In Table I we report the parameters of our simulations performed with the random-exchange algorithm: here $N_{\rm run}$ is the number of Metropolis sweeps per sample and temperature, while $N_{\rm therm}$ is the corresponding number of Metropolis sweeps discarded for thermalization. We also report the range of the exchange probability, which depends on the temperatures β_i and β_{i+1} considered.

For every disorder sample we perform a MC run of $N_{\rm run}$ Metropolis iteration collecting $N_{\rm meas}$ measures of the quantities defined in the Appendix. We used $N_{\rm meas}=400$ for $L\le 24$ and $N_{\rm meas}=100$ for $L\ge 32$. In order to obtain equilibrated data, we discard a fraction of the measures which is determined by using the following procedure. We divide the measures into N_B parts (typically $N_B=10,20$) of length $l=N_{\rm meas}/N_B$. Then, we consider the disorder-averaged susceptibilities

$$\chi_b(t)=\left[\frac{1}{l}\sum_{i=tl}^{(t+1)l-1}\chi(i)\right], \quad t=0,\ldots,N_B-1. \tag{21}$$

Starting from random infinite-temperature spin configurations, $\chi_b(t)$ increases with t. When t is sufficiently large, $\chi_b(t)$ becomes constant within error bars, thus signaling that thermalization has been reached. We use the susceptibility because it is a long-range quantity and it is more sensitive to thermalization. Whenever one determines disorder averages of functions of thermal averages one should perform a bias correction; for this purpose we use the results of Ref. [47].

MC results are reported in Tables II and III. To obtain small statistical errors, we generate a large number of samples N_s: $N_s=10^6$ in all cases, except for the run with $L=32$ and $p=0.891$, where $N_s=4\times 10^6$. To check the computer programs we used the exact prediction of the energy density along the N line [38],

TABLE III. MC data for $L=24$, 32, 48, and 64 along the N line. The number of samples is $N_s=10^6$, except for the run with $L=32$ and $p=0.891$. In this case $N_s=4\times10^6$.

L	p	R_ξ	U_4	U_{22}	χ	R'_ξ
24	0.8895	0.9423(7)	1.1411(2)	0.09071(18)	321.10(10)	182.16(12)
	0.889972	0.9615(7)	1.1356(2)	0.08730(17)	324.95(9)	179.74(11)
	0.8905	0.9831(7)	1.1299(2)	0.08373(16)	329.20(9)	176.77(11)
	0.891	1.0042(7)	1.1247(2)	0.08054(16)	333.15(9)	173.76(11)
	0.8915	1.0265(8)	1.1194(2)	0.07724(15)	337.14(10)	170.92(11)
	0.892	1.0486(8)	1.1145(2)	0.07412(15)	341.06(9)	168.12(10)
32	0.8895	0.9319(6)	1.1443(2)	0.09279(18)	538.29(16)	351.4(3)
	0.889972	0.9533(7)	1.1380(2)	0.08878(18)	546.13(17)	346.3(3)
	0.8905	0.9808(7)	1.1306(2)	0.08423(17)	555.14(17)	334.0(3)
	0.891	1.0058(4)	1.12439(10)	0.080358(8)	563.43(8)	334.02(14)
	0.8915	1.0315(8)	1.1184(2)	0.07651(16)	571.52(16)	328.6(3)
	0.892	1.0587(8)	1.11249(18)	0.07292(15)	579.70(16)	322.2(2)
48	0.889972	0.9430(7)	1.1413(2)	0.09079(17)	1134.1(3)	864.7(8)
	0.8905	0.9758(7)	1.1321(2)	0.08498(17)	1158.4(3)	847.8(8)
	0.891	1.0088(7)	1.1237(2)	0.07984(16)	1181.8(3)	830.2(7)
	0.8915	1.0438(8)	1.11581(18)	0.07487(15)	1204.9(3)	814.2(7)
64	0.889972	0.9311(6)	1.1449(2)	0.09308(17)	1900.0(6)	1641.3(1.6)
	0.8906	0.9792(7)	1.1313(2)	0.08460(17)	1961.0(6)	1596.9(1.6)
	0.8909	1.0037(7)	1.1252(2)	0.08072(17)	1990.3(6)	1580.2(1.5)
	0.8912	1.0286(8)	1.1194(2)	0.07711(16)	2019.1(6)	1560.2(1.6)

$$E_N(p) = \frac{1}{V}[\langle \mathcal{H} \rangle_{T_N(p)}] = 2 - 4p. \tag{22}$$

All runs give estimates of $E_N(p)$ which are consistent with Eq. (22). For example, we obtain $E_N(p)/(2-4p) = 1.000\,01(1), 1.000\,00(1)$ for $L=32$, $p=0.891$ and $L=64$, $p=0.8909$, respectively.

B. Results

MC estimates of the RG invariant quantities R_ξ, U_4, and U_{22} along the N line are shown in Fig. 2. There is clearly a crossing point at $p \approx 0.891$. The raw data already indicate that $p^* > p_e = 0.889\,972\ldots$, where p_e is the value conjectured in Ref. [17]. Their difference can hardly be explained in terms of scaling corrections. Indeed, the crossing point $p_{\rm cross}(L,\alpha)$ of the data corresponding to lattice sizes L and αL scales for $L\to\infty$ as

$$p_{\rm cross}(L,\alpha) - p^* \sim L^{-y_1-\omega}, \tag{23}$$

where $\omega > 0$ is the exponent associated with the leading irrelevant operator. Since, as we shall see, $y_1 \approx 0.6$, the approach is reasonably fast, so that our data, that correspond to lattice sizes between 6 and 64, should be able to detect a drift due to scaling corrections. The very good stability of the results excludes a delayed approach to p_e.

In order to estimate precisely p^*, T^*, and y_1 we perform a FSS analysis of the phenomenological couplings $R_\xi \equiv \xi/L$, U_4, U_{22}, and U_d, which are defined in the Appendix and are generically denoted by R. Since we vary p and β along the N line, close to the MNP we expect

$$R = f_R[(p-p^*)L^{y_1}], \tag{24}$$

with $f_R(0)=R^*$. This functional form relies on the property that $u_2=0$ along the N line. Since our data are sufficiently close to the MNP, the product $(p-p^*)L^{y_1}$ is small. We can thus expand $f_R(x)$ in powers of x. Thus we fit the numerical data to

$$R = R^* + \sum_{n=1}^{n_{\rm max}} a_n (p-p^*)^n L^{n y_1}, \tag{25}$$

keeping R^*, the coefficients $\{a_n\}$, p^*, and y_1 as free parameters. Here we neglect scaling corrections. To monitor their role, we repeat the fits several times, each time only including data satisfying $L \geq L_{\rm min}$. Fits with $n_{\rm max}=1$ have a large $\chi^2/{\rm DOF}$ (DOF is the number of degrees of freedom of the fit), indicating that the range of values of p we are considering is too large to allow for a linear approximation of the scaling function $f_R(x)$. Fits with $n_{\rm max}=2$ have instead a good χ^2 for $L_{\rm min} \geq 6$ (U_4), 12 (R_ξ), and 16 (U_{22} and U_d). We also perform fits with $n_{\rm max}=3$ but we do not observe significant differences: for U_d and $L_{\rm min}=6,12$ we obtain $\chi^2/{\rm DOF} = 2148/39, 34/27$ with $n_{\rm max}=2$, and 2147/38,34/26 for $n_{\rm max}=3$. Clearly, a parabolic approximation is fully adequate. Beside fitting separately each observable, we also perform combined fits of three different phenomenological couplings. The results are reported in Table IV. In the case of U_{22}, U_4, and

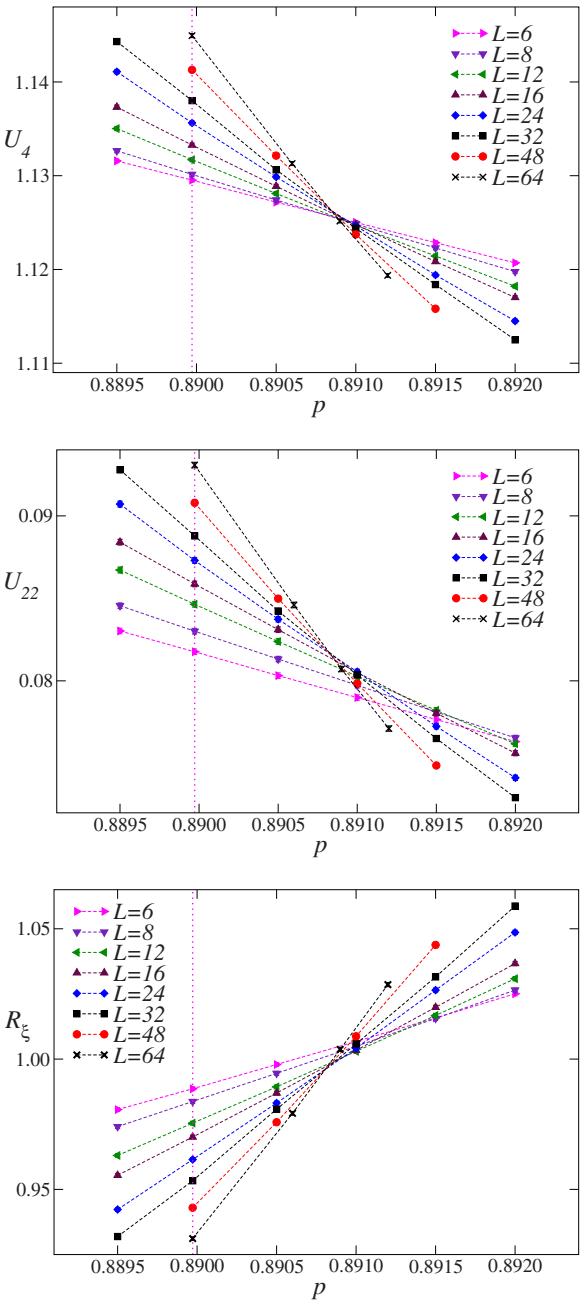

FIG. 2. (Color online) MC data of U_4, U_{22}, and $R_\xi \equiv \xi/L$ vs p. The dashed lines connecting the data at given L are drawn to guide the eye. The dotted vertical line corresponds to the conjectured [17] MNP location $p=p_e=0.889\,972$.

R_ξ all estimates of p^* show a systematic downward trend with $L_{\min}$, with $0.890\,80 \lesssim p^* \lesssim 0.890\,83$ for $L_{\min}=32$. Fits of U_d (note that this quantity is statistically more precise than the other ones, which explains the somewhat larger χ^2/DOF of the fits) show instead a different behavior and suggest a somewhat larger value of p^*, $p^* \approx 0.890\,87$. Similar trends are observed in the estimates of y_1, which in most of the cases increases with $L_{\min}$ and varies essentially in the range $0.65 \lesssim y_1 \lesssim 0.67$ with a statistical error of $\pm 0.01-0.02$.

These tiny discrepancies indicate that scaling corrections are not negligible if compared with our small statistical errors. In order to estimate their quantitative role, we also perform fits in which scaling corrections are taken into account. Thus we fit the MC data to

$$R = R^* + \sum_{n=1}^{n_{\max}} a_n (p-p^*)^n L^{n y_1} + L^{-\omega} \sum_{k=0}^{k_{\max}} b_k (p-p^*)^k L^{k y_1}. \tag{26}$$

Results for $k_{\max}=0$ and 1 have both a good χ^2/DOF, even for $L_{\min}=6$. In the following we present results corresponding to $k_{\max}=1$, since this choice allows us to take into account the scaling corrections that affect the determination of both p^* and y_1. The correction-to-scaling exponent ω is not known and thus we keep it as a free parameter. Our results are reported in Table V. Because of the large number of parameters this fit gives stable results only for $L_{\min}=6,8$ (for U_4 this is not even the case). For larger values of $L_{\min}$ errors are so large to make the results meaningless. The results are fully consistent. First of all, they predict $\omega \gtrsim 1$. Thus corrections to scaling decay reasonably fast, indicating that the systematic error should be reasonably estimated by considering data in our range $6 \le L \le 64$. Second, fits that involve U_d give

TABLE IV. Estimates of p^* and y_1 obtained by performing a fit to Eq. (25) with $n_{\max}=2$. DOF is the number of degrees of freedom in the fit and $L_{\min}$ is the minimum lattice size included in the fit.

	$L_{\min}$	χ^2/DOF	p^*	y_1
U_d	12	34/27	0.890860(7)	0.658(7)
	16	19/21	0.890877(8)	0.656(9)
	24	17/15	0.890881(11)	0.647(11)
	32	14/9	0.890871(14)	0.664(16)
U_{22}	12	41/27	0.890895(12)	0.639(11)
	16	11/21	0.890857(13)	0.647(13)
	24	6/15	0.890831(17)	0.663(18)
	32	3/9	0.890813(21)	0.672(25)
U_4	12	19/27	0.890882(9)	0.647(9)
	16	9/21	0.890865(10)	0.650(10)
	24	6/15	0.890850(13)	0.656(14)
	32	3/9	0.890834(17)	0.669(19)
R_ξ	12	21/27	0.890835(8)	0.647(8)
	16	12/21	0.890820(9)	0.650(9)
	24	7/15	0.890805(12)	0.653(12)
	32	5/9	0.890795(15)	0.664(17)
R_ξ, U_4, U_{22}	12	107/85	0.890864(5)	0.646(5)
	16	44/67	0.890844(6)	0.650(6)
	24	27/49	0.890826(8)	0.656(8)
	32	14/31	0.890812(10)	0.668(11)
R_ξ, U_4, U_d	12	92/85	0.890858(4)	0.651(4)
	16	64/67	0.890855(5)	0.653(5)
	24	54/49	0.890847(7)	0.652(7)
	32	37/31	0.890836(9)	0.665(10)

TABLE V. Estimates of p^*, y_1, and ω obtained by performing a fit to Eq. (26) with $n_{\max}=2$ and $k_{\max}=1$. DOF is the number of degrees of freedom in the fit and $L_{\min}$ is the minimum lattice size included in the fit.

	$L_{\min}$	χ^2/DOF	p^*	y_1	ω
ξ/L	6	9.9/36	0.89077(2)	0.663(16)	1.18(31)
	8	7.3/30	0.89079(2)	0.654(13)	1.95(68)
U_{22}	6	7.6/36	0.89077(3)	0.663(21)	1.23(25)
	8	7.1/30	0.89078(4)	0.660(23)	1.45(46)
U_d	6	31/36	0.89090(1)	0.655(8)	2.67(16)
	8	20/30	0.89088(1)	0.654(8)	4.15(68)
$\xi/L,U_4,U_{22}$	6	77/114	0.89082(1)	0.657(8)	1.59(17)
	8	47/96	0.89081(1)	0.657(10)	1.64(32)
$\xi/L,U_4,U_d$	6	128/114	0.890868(5)	0.652(5)	3.04(12)
	8	81/96	0.890860(5)	0.651(5)	5.25(71)

estimates of ω that are significantly larger. This is consistent with the results reported in Table V: fits involving U_d show a small dependence on $L_{\min}$, suggesting that U_d is less affected by scaling corrections. The estimates of p^* obtained in fits of ξ/L and U_{22} show a trend that is opposite to that observed in fits without corrections, indicating that the correct value for p^* belongs to the range of values that occur in the two types of fits: values smaller than 0.890 70 are not consistent with our data. To quote a final result, let us note that the fits with $L_{\min}=8$ reported in Table V give (including the statistical error) $0.890\,74 \lesssim p^* \lesssim 0.890\,89$. A conservative estimate is therefore

$$p^* = 0.890\,81(7). \tag{27}$$

This result is fully consistent with those obtained in the fits without scaling corrections. Using Eq. (3) we obtain

$$\beta^* = 1.0495(4), \quad T^* = 0.9528(4). \tag{28}$$

Note that the conjectured value [17] $p_e=0.889\,972\ldots$ is excluded, the difference $p^*-p_e=0.000\,84(7)$ corresponding to 12 error bars.

Let us finally estimate y_1. Fits with scaling corrections give results that decrease with $L_{\min}$, while fits without scaling corrections give estimates that have the opposite trend. Comparing all results, we expect $0.64 \lesssim y_1 \lesssim 0.67$, so that we arrive at the final estimate

$$y_1 = 0.655(15). \tag{29}$$

The fits that we have reported also allow us to estimate the critical-point value R^* of the phenomenological couplings. We obtain:

$$R_\xi^* = 0.996(2), \tag{30}$$

$$U_4^* = 1.1264(6), \tag{31}$$

$$U_{22}^* = 0.0817(5), \tag{32}$$

$$U_d^* = 1.0447(3). \tag{33}$$

Of course, the estimate of U_d^* is consistent with the relation $U_d^*=U_4^*-U_{22}^*$. Note that these results are not very much different from those of the pure 2D Ising values that apply along the PF line from the pure Ising point at $p=1$ to the MNP [48]: $R_\xi^*=0.905\,048\,829\,2(4)$, $U_4^*=U_d^*=1.167\,923(5)$, $U_{22}^*=0$. In particular, the estimate (32) of U_{22}^* is quite small, indicating that the violations of self-averaging are small.

Let us now consider the derivatives R' of the phenomenological couplings. Close to the MNP, R' is expected to behave as

$$R' = L^{\zeta} f_{R'}[(p-p^*)L^{y_1}], \tag{34}$$

where we have used the fact that along the Nishimori line $u_2=0$. If Eq. (11) holds [37], we have additionally $\zeta=y_2$. To determine ζ we perform analyses analogous to those used before to determine p^* and y_1. We expand $f_{R'}(x)$ in powers of x and thus fit R' to

$$\ln R' = \zeta \ln L + \sum_{n=0}^{n_{\max}} a_n (p-p^*)^n L^{n y_1}. \tag{35}$$

We always fix y_1 to the value (29) and p^* to the value (27), including in the final error the variation of y_1 and p^* within one error bar. As in the fits of R, we check the role of $n_{\max}$. A significant improvement in the quality of the fit is observed by changing $n_{\max}$ from 1 to 2, while no significant change is obtained by increasing it to 3. Therefore we fix $n_{\max}=2$.

The results are reported in Table VI. They are very stable and show a very small dependence on $L_{\min}$, of the order of the statistical error. As a final result we quote $\zeta=0.250(2)$. This result is significantly smaller than y_1 and thus confirms the argument of Ref. [37]. Therefore ζ should be identified with y_2, so that

$$y_2 = 0.250(2), \quad \nu \equiv \frac{1}{y_2} = 4.00(3). \tag{36}$$

The corresponding crossover exponent is

TABLE VI. Estimates of the exponent $\zeta=y_2$ and $\zeta=\eta$ obtained by performing a fit to Eq. (35) with $n_{\max}=2$.

	$L_{\min}$	χ^2/DOF	ζ
R'_ξ	8	20/29	0.252(2)
	12	16/24	0.251(2)
	16	13/19	0.250(2)
	24	12/14	0.249(3)
U'_4	8	19/29	0.250(1)
	12	17/24	0.249(1)
	16	14/19	0.249(1)
	24	13/14	0.250(2)
Z	8	147/29	0.173(3)
	12	38/24	0.175(3)
	16	21/19	0.176(4)
	24	11/14	0.178(5)
	32	6/9	0.179(5)

$$\phi \equiv \frac{y_1}{y_2} = 2.62(6). \tag{37}$$

The same analysis used to estimate y_2 can be employed to determine η. Instead of χ, we consider

$$Z \equiv \chi/\xi^2 \sim L^{-\eta}, \tag{38}$$

which has smaller statistical errors. We fit Z to

$$\ln Z = -\eta \ln L + \sum_{n=0}^{n_{\max}} a_n (p-p^*)^n L^{n y_1}. \tag{39}$$

As before, we fix y_1 and p^*, set $n_{\max}=2$, and repeat the fit several times, each time considering only data satisfying $L \geq L_{\min}$. The final results are reported in Table VI. A good χ^2 is obtained only for $L_{\min} \geq 16$. The corresponding fits give $\eta \approx 0.175-0.180$ with a slight upward trend. This effect may be real and due to scaling corrections. Therefore we also fit $\ln Z$ to

$$\ln Z = -\eta \ln L + \sum_{n=0}^{n_{\max}} a_n (p-p^*)^n L^{n y_1} + L^{-\omega} \sum_{k=0}^{k_{\max}} a_k (p-p^*)^k L^{k y_1}, \tag{40}$$

fixing y_1 and p^*, and keeping ω as a free parameter. For $n_{\max}=2$ and $k_{\max}=1$, we obtain a good χ^2 for any $L_{\min} \geq 6$. The corresponding estimates of η are $\eta=0.182(10)$ ($L_{\min}=6$) and $\eta=0.181(10)$ ($L_{\min}=8$). The central estimates are quite close to those obtained in fits without scaling corrections, indicating that scaling corrections are small. We take as our final estimate

$$\eta = 0.180(5), \tag{41}$$

which includes all results without scaling corrections and is consistent with the fits in which scaling corrections are taken into account.

IV. CONCLUSIONS

In this paper we investigated the critical behavior of the square-lattice $\pm J$ Ising model close to the MNP. Our main results are the following.

(i) We obtained an accurate estimate of the location of the MNP: $p^*=0.890\,81(7)$, $T^*=0.9528(4)$. The conjectured value $p_e=0.889\,972\ldots$ put forward in Ref. [17] is a very good approximation, but it is not exact: $p^*-p_e=0.000\,84(7)$.

(ii) We computed the RG dimensions of the relevant operators at the MNP, obtaining $y_1=0.655(15)$ and $y_2=0.250(2)$. It is tempting to conjecture that $y_2=1/4$ exactly. Note also that y_1 is consistent with 2/3, though in this case the precision of the result is not good enough to put this conjecture on firm grounds. The above estimates of the RG dimensions give $\nu \equiv 1/y_2=4.00(3)$ and $\phi \equiv y_1/y_2=2.62(6)$.

(iii) We computed the critical exponent η that controls the critical behavior of the magnetic correlations, obtaining $\eta=0.180(5)$.

Our estimate of p^* is significantly more precise than those obtained in previous works. By using transfer-matrix methods Refs. [16,18,20,28] obtained $p^*=0.8907(2)$, 0.8906(2), 0.8905(5), 0.889(2), respectively. We also mention the results $p^*=0.8872(8)$ obtained by means of an off-equilibrium MC simulation [21], and $p^*=0.886(3)$ from the analysis of high-temperature expansions [25]. Concerning the critical exponents at the MNP, we mention the square-lattice results $y_1=0.676(14)$, 0.667(13), 0.752(17), 0.75(7), 0.76(5), respectively, from Refs. [10,16,18,2,25]. The estimate [11] $y_1=0.671(9)$ has been obtained on the triangular and honeycomb lattices. Moreover, we mention the result [10] $y_1=0.658(13)$ obtained from a model with Gaussian distributed couplings. The most recent results are clearly consistent with our estimate. As for y_2 (or equivalently $\nu=1/y_2$), Refs. [10,16,2] report $\nu \approx 3$, $\nu=4.0(5)$, and $\nu=2.4(3)$, which are not far from our much more precise result (but the old result of Ref. [2] is clearly inconsistent with the quoted errors). Finally, we quote $\eta=0.183(3)$ [16], and $\eta=0.1848(3), 0.1818(2)$, (statistical errors only) obtained in Ref. [10], respectively, for the $\pm J$ model and for the model with Gaussian distributed couplings. They are fully consistent with our result.

It is interesting to compare the phase diagram of the two-dimensional $\pm J$ Ising model, shown in Fig. 1, with that of the three-dimensional $\pm J$ Ising model sketched in Fig. 3. Recent high-statistics numerical studies of the $\pm J$ Ising model on a simple cubic lattice have shown that: (i) the transitions along the PF line belong to the 3D randomly dilute Ising (RDI) universality class [44], with critical exponents [47] $\nu=0.683(2)$ and $\eta=0.036(1)$; (ii) this line extends up to a magnetic-glassy multicritical point (MGP) located along the N line, at [42] $p^*=0.768\,20(4)$, where the relevant RG dimensions are given by $y_1=1.02(5)$ and $y_2=0.61(2)$ [corresponding to the thermal and crossover exponents $\nu=1.64(5)$ and $\phi=1.67(10)$]; (iii) the critical behavior along the transition line separating the paramagnetic and the spin-glass phase is independent of p and belongs to the Ising spin-glass universality class [49] with the correlation-length critical exponent $\nu=2.53(8)$.

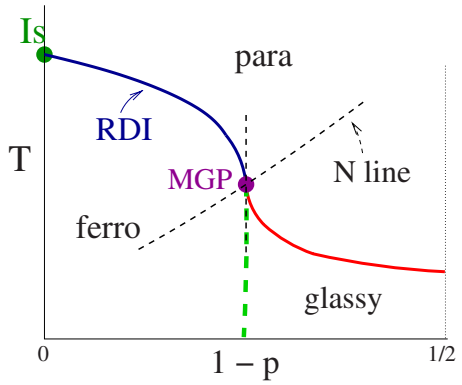

FIG. 3. (Color online) Phase diagram of the 3D $\pm J$ Ising model in the T-p plane.

APPENDIX: NOTATIONS

The two-point correlation function is defined as

$$G(x) \equiv [\langle \sigma_0 \sigma_x \rangle], \tag{A1}$$

where the angular and the square brackets indicate, respectively, the thermal average and the quenched average over disorder. We define the magnetic susceptibility $\chi \equiv \Sigma_x G(x)$ and the correlation length ξ,

$$\xi^2 \equiv \frac{\tilde{G}(0) - \tilde{G}(q_{\min})}{\hat{q}^2_{\min} \tilde{G}(q_{\min})}, \tag{A2}$$

where $q_{\min} \equiv (2\pi/L, 0)$, $\hat{q} \equiv 2 \sin q/2$, and $\tilde{G}(q)$ is the Fourier transform of $G(x)$. We also consider quantities that are invariant under RG transformations in the critical limit. Besides the ratio

$$R_\xi \equiv \xi/L, \tag{A3}$$

we consider the quartic cumulants

$$U_4 \equiv \frac{[\mu_4]}{[\mu_2]^2},$$

$$U_{22} \equiv \frac{[\mu_2^2] - [\mu_2]^2}{[\mu_2]^2},$$

$$U_d \equiv U_4 - U_{22},$$

where

$$\mu_k \equiv \left\langle \left(\sum_x \sigma_x \right)^k \right\rangle. \tag{A4}$$

The quantities R_ξ, U_4, U_{22}, and U_d are also called phenomenological couplings. Finally, we consider the derivatives

$$R'_\xi \equiv \frac{dR_\xi}{d\beta}, \quad U'_4 \equiv \frac{dU_4}{d\beta}, \tag{A5}$$

which can be computed by measuring appropriate expectation values at fixed β and p.

[1] S. F. Edwards and P. W. Anderson, J. Phys. F: Met. Phys. **5**, 965 (1975).
[2] S. Cho and M. P. A. Fisher, Phys. Rev. B **55**, 1025 (1997).
[3] I. A. Gruzberg, N. Read, and A. W. W. Ludwig, Phys. Rev. B **63**, 104422 (2001).
[4] J. T. Chalker, N. Read, V. Kagalovsky, B. Horovitz, Y. Avishai, and A. W. W. Ludwig, Phys. Rev. B **65**, 012506 (2001).
[5] C. Wang, J. Harrington, and J. Preskill, Ann. Phys. (N.Y.) **303**, 31 (2003).
[6] A. Kitaev, Ann. Phys. (N.Y.) **303**, 2 (2003).
[7] E. Dennis, A. Kitaev, A. Landahl, and J. Preskill, J. Math. Phys. **43**, 4452 (2002).
[8] H. Nishimori, *Statistical Physics of Spin Glasses and Information Processing: An Introduction* (Oxford University Press, Oxford, 2001).
[9] H. Nishimori, J. Stat. Phys. **126**, 977 (2007).
[10] M. Picco, A. Honecker, and P. Pujol, J. Stat. Mech.: Theory Exp. (2006) P09006.
[11] S. L. A. de Queiroz, Phys. Rev. B **73**, 064410 (2006).
[12] C. Amoruso and A. K. Hartmann, Phys. Rev. B **70**, 134425 (2004).
[13] N. Kawashima and H. Rieger, in *Frustrated Spin Systems*, edited by H. T. Diep (World Scientific, Singapore, 2004).
[14] S. L. A. de Queiroz and R. B. Stinchcombe, Phys. Rev. B **68**, 144414 (2003).
[15] J. M. Maillard, K. Nemoto, and H. Nishimori, J. Phys. A **36**, 9799 (2003).
[16] F. Merz and J. T. Chalker, Phys. Rev. B **65**, 054425 (2002).
[17] H. Nishimori and K. Nemoto, J. Phys. Soc. Jpn. **71**, 1198 (2002).
[18] A. Honecker, M. Picco, and P. Pujol, Phys. Rev. Lett. **87**, 047201 (2001).
[19] F. D. Nobre, Phys. Rev. E **64**, 046108 (2001).
[20] F. D. A. Aarão Reis, S. L. A. de Queiroz, and R. R. dos Santos, Phys. Rev. B **60**, 6740 (1999).
[21] Y. Ozeki and N. Ito, J. Phys. A **31**, 5451 (1998).
[22] J. A. Blackman, J. R. Goncalves, and J. Poulter, Phys. Rev. E **58**, 1502 (1998).
[23] G. Migliorini and A. N. Berker, Phys. Rev. B **57**, 426 (1998).
[24] N. Kawashima and H. Rieger, Europhys. Lett. **39**, 85 (1997).
[25] R. R. P. Singh and J. Adler, Phys. Rev. B **54**, 364 (1996).
[26] Y. Ozeki and H. Nishimori, J. Phys. A **26**, 3399 (1993).
[27] H. Kitatani, J. Phys. Soc. Jpn. **61**, 4049 (1992).
[28] Y. Ozeki and H. Nishimori, J. Phys. Soc. Jpn. **56**, 3265 (1987).
[29] H. Nishimori, J. Phys. Soc. Jpn. **55**, 3305 (1986).
[30] B. N. Shalaev, Sov. Phys. Solid State **26**, 1811 (1984).
[31] R. Shankar Phys. Rev. Lett. **58**, 2466 (1987); **59**, 380(E) (1987); A. W. W. Ludwig, *ibid.* **61**, 2388 (1988); H. A. Ceccatto and C. Naon, *ibid.* **61**, 2389 (1988).
[32] H. G. Ballesteros, L. A. Fernández, V. Martín-Mayor, A.

Muñoz Sudupe, G. Parisi, and J. J. Ruiz-Lorenzo, J. Phys. A **30**, 8379 (1997).
[33] M. Hasenbusch, F. Parisen Toldin, A. Pelissetto, and E. Vicari, e-print arXiv:0804.2788.
[34] A. W. W. Ludwig and J. L. Cardy, Nucl. Phys. B **285**, 687 (1987); J. L. Cardy J. Phys. A **19**, L1093 (1986); **20**, 5039(E) (1987).
[35] A. Georges, D. Hansel, P. Le Doussal, and J. Bouchaud, J. Phys. (Paris) **46**, 1827 (1985).
[36] P. Le Doussal and A. B. Harris, Phys. Rev. Lett. **61**, 625 (1988).
[37] P. Le Doussal and A. B. Harris, Phys. Rev. B **40**, 9249 (1989).
[38] H. Nishimori, Prog. Theor. Phys. **66**, 1169 (1981).
[39] T. Jörg, J. Lukic, E. Marinari, and O. C. Martin, Phys. Rev. Lett. **96**, 237205 (2006); C. Amoruso, E. Marinari, O. C. Martin, and A. Pagnani, *ibid.* **91**, 087201 (2003).
[40] M. Ohzeki, H. Nishimori, and A. N. Berker, e-print arXiv:0802.2760.
[41] M. Hinczewski and A. N. Berker, Phys. Rev. B **72**, 144402 (2005).
[42] M. Hasenbusch, F. P. Toldin, A. Pelissetto, and E. Vicari, Phys. Rev. B **76**, 184202 (2007).
[43] R. R. P. Singh, Phys. Rev. Lett. **67**, 899 (1991).
[44] M. Hasenbusch, F. P. Toldin, A. Pelissetto, and E. Vicari, Phys. Rev. B **76**, 094402 (2007).
[45] C. J. Geyer, in *Computer Science and Statistics: Proc. of the 23rd Symposium on the Interface*, edited by E. M. Keramidas (Interface Foundation, Fairfax Station, 1991), p. 156; K. Hukushima and K. Nemoto, J. Phys. Soc. Jpn. **65**, 1604 (1996).
[46] F. Parisen Toldin, A. Pelissetto, and E. Vicari, J. Stat. Mech.: Theory Exp. (2006) P06002.
[47] M. Hasenbusch, F. Parisen Toldin, A. Pelissetto, and E. Vicari, J. Stat. Mech.: Theory Exp. (2007) P02016.
[48] J. Salas and A. D. Sokal, J. Stat. Phys. **98**, 551 (2000).
[49] M. Hasenbusch, A. Pelissetto, and E. Vicari, J. Stat. Mech.: Theory Exp. (2008) L02001.